Ultradipole photon production in 40 and 50 MeV α-nucleus collisions

M. K. Sharan, Y. K. Agarwal, and C. V. K. Baba
Tata Institute of Fundamental Research, Bombay 400 005, India

D. R. Chakrabarty and V. M. Datar
Nuclear Physics Division, Bhabha Atomic Research Centre, Bombay 400 085, India
(Received 4 June 1993)

γ-ray yields in the energy range ~5–35 MeV have been measured in the reactions $\alpha + {}^{197}$Au and ^{159}Tb at E_α=40 MeV and $\alpha + {}^{197}$Au, ^{116}Sn, ^{nat}Ag, and ^{59}Co at E_α=50 MeV at $\theta_\gamma = 90°$. Angular distribution measurements have been carried out for the heaviest and the lightest targets at E_α = 50 MeV. A reasonably good agreement with the statistical model calculations is obtained for photon energies up to the giant dipole resonance region. A nonstatistical component is observed at higher γ-ray energies for all the systems studied. An attempt to understand the production mechanism of the nonstatistical part is made in terms of the potential bremsstrahlung and the incoherent nucleon-nucleon bremsstrahlung processes. While the calculations give the right order of magnitude of the measured cross sections for the highest γ-ray energies, they fail to reproduce the measured angular distributions and the cross sections in the entire γ-ray energy range.

PACS number(s): 25.55.−e, 24.30.Cz

I. INTRODUCTION

There are many studies, both experimental and theoretical, on high energy γ-ray production following heavy-ion and α-particle bombardment on nuclei [1–6]. The photon production mechanism in low energy heavy-ion collisions ($E/A \lesssim 8$ MeV) has been well understood in terms of the statistical decay of an excited compound nucleus after incorporating the isovector giant dipole resonance (GDR) built on excited nuclear states. In collisions involving higher projectile energies, an excess of photon yield over that expected on the basis of the statistical model has been observed, especially for γ-ray energies exceeding the GDR region. This "nonstatistical" yield has been referred [7] to as ultradipole radiation (UDR) and has been understood in terms of incoherent nucleon-nucleon collisional bremsstrahlung [1–3,7,8] with reasonable success, particularly, for beam energies of E/A >20 MeV. Other mechanisms like nucleus-nucleus bremsstrahlung [9,10], statistical decay of a thermally equilibrated fireball [8], and clusters [11] have been proposed for explaining the UDR but seem to be less successful. Only a few experiments [12–15] have been reported at beam energies between 10 and 20 MeV/nucleon and the nucleon-nucleon bremsstrahlung model generally underestimates the UDR yield observed in these cases.

Alpha-induced UDR has been studied by Tam *et al.* [16] at E_α =100 and 212 MeV on several targets. These data can be understood to within factors of 3 on the basis of nucleon-nucleon bremsstrahlung models. At low α energies, significant UDR yields have been observed in 27 MeV α+^{154}Sm [4] and 28 MeV α+^{59}Co [17] reactions, unlike the situation with heavier projectiles at similar beam energies per nucleon. Nakayama and Bertsch [18] attempted to explain the α+^{154}Sm data in terms of nucleus-nucleus potential bremsstrahlung as well as nucleon-nucleon bremsstrahlung. The latter model underpredicts the data by factors of up to 10, but is successful in reproducing the energy dependence of the UDR yield. The potential bremsstrahlung model reproduces the observed cross sections only near the kinematic limit and underpredicts the data at lower photon energies. An improved version of their nucleon-nucleon bremsstrahlung model [19] which includes the nucleon and γ-ray energy-dependent T matrices seems to explain the 10 MeV/nucleon ^{12}C+^{154}Sm data [4], but has not been applied specifically to the low-energy α-induced reactions.

In order to understand the production mechanism of UDR, particularly the role of potential and nucleon-nucleon bremsstrahlung following α-induced reactions at low bombarding energies, we have measured γ-ray yields for $E_\gamma \sim$ 5 to 35 MeV for several targets at E_α =40 and 50 MeV both in the singles mode and in coincidence with a set of γ-ray multiplicity detectors. Angular distribution measurements were made in some of the cases. The data have been compared to the calculations based on potential bremsstrahlung and the first chance nucleon-nucleon bremsstrahlung model *à la* Nakayama and Bertsch [7,19] with realistic momentum distributions of nucleons in the projectile and the target. The experimental details are presented in Sec. II. In Sec. III we present the experimental data along with the statistical model analysis for the lower energy part of the γ-ray spectrum. In Sec. IV an attempt to understand the UDR cross sections in terms of bremsstrahlung models is described. A summary is given in Sec. V.

II. EXPERIMENTAL DETAILS

The experiments were carried out at the Variable Energy Cyclotron Centre, Calcutta, using α beams of 40

and 50 MeV, bombarding self-supporting metallic targets of ^{197}Au, ^{159}Tb, ^{116}Sn (isotopically enriched to 98%), ^{nat}Ag, and ^{59}Co. The details regarding the reactions studied are listed in Table I. The typical beam current used was $\sim$ 1 nA (electrical). γ rays were measured in the energy range of $\sim$ 5 to 35 MeV in an array of seven 15 cm thick, closely packed regular hexagonal NaI(Tl) detectors, each inscribed in a circle of 7.5 cm radius. The detector assembly was placed at 90° at a distance of 100 cm from the target, subtending a solid angle of 0.9% of 4π. For angular distribution studies additional measurements were made at 45° and 135° for ^{197}Au and ^{59}Co targets at E_α =50 MeV. The detectors were surrounded by anti-coincidence plastic scintillators (50×50×5 cm^3) on the sides and the top to veto the cosmic ray muons. The NaI(Tl) detectors and plastic scintillator assembly was shielded against background γ rays by a $\sim$10 cm thick layer of lead placed on the sides and the top. A 5 mm thick lead sheet in front of the detector assembly was used to reduce the count rate due to low energy γ rays and x rays produced in the target. The detector array was further covered on the sides by boric acid to reduce the thermal neutron background. In addition, four 5.1 cm ϕ×5.1 cm NaI(Tl) detectors were placed at a distance of $\sim$8 cm from the target and were operated in coincidence with the main detector array giving information about the mean γ-ray multiplicity associated with each event.

The response of the detector assembly was measured at γ-ray energies of 6.14, 10.76, 12.84, 17.27, 24.4, and 28.8 MeV in auxiliary experiments using proton induced reactions on ^{19}F, ^{27}Al, and ^{11}B. The response was also calculated using the EGS4 [20] code and a good agreement (within 10%) was found with the measurements and hence the calculated response was used to fold or unfold the γ-ray spectra. During the main experiment the calibration and the stability were checked using the E_γ =4.43 MeV line from a Ra-Be source, and E_γ =6.83 MeV peak from the thermal neutron capture in iodine in each of the seven NaI(Tl) detectors. The data were recorded in list mode using a CAMAC based data acquisition system [21]. The four parameters measured for each event were (1) the total energy (E) deposited in the main detector array, (2) time difference [time of flight (TOF)] between the fast signal from the main detector (time matched OR of the seven detectors) and the cyclotron r.f. signal, (3) pileup parameter (P) derived from the zero crossover time of the total energy (bipolar) pulse, and (4) the time difference between the time matched fast OR of the trigger detectors and the main detector. The TOF spectra were projected for $\sim$0.5 MeV bins in E with the appropriate gate on P. The time resolution for the prompt photons was $\sim$3 ns for $E_\gamma \gtrsim$8 MeV. Typical TOF spectra from the 50 MeV α+^{197}Au runs for $\langle E \rangle$ $\sim$20 and 30 MeV are shown in Fig. 1. It is clear that the fast neutrons are well separated from the prompt γ rays up to the highest energies measured. A suitable gate was set on the parameter P to minimize the pileup events and the residual pileup (within the gate) was corrected for by an extrapolation procedure. This method of pileup rejection was tested by comparing the cross sections derived from two separate runs on ^{197}Au target at E_α=40 MeV, with beam currents of 0.5 and 2 electrical nA. The results agreed within 10% of each other throughout the γ-ray energy region. The NaI(Tl) detectors also showed moderate pulse shape discrimination for $E \gtrsim$ 15 MeV which enabled additional neutron rejection with an appropriate choice of the P gate.

The neutron background from the beam dump situated at 2.5 m from the target was minimized by surrounding it with a tank (1 m×1 m×1 m) containing a solution of boric acid in water, paraffin blocks, and lead. In order to reduce background from beam halo interaction with the target frame, large area targets ($\sim$30 mm×30 mm) supported only from the top were used. For γ-ray energies from 10 to 25 MeV, an estimate of the background contribution was made (a) by placing a 10 cm thick lead in front of the target and (b) by placing a blank frame in the target position. In both the cases the background

TABLE I. List of the reactions studied. E_{beam} is the beam energy, T is the target thickness, P is the target purity, and E^* is the average excitation energy in the compound nucleus.

Reaction	E_{beam} (MeV)	T (mg/cm^2)	P (%)	E^* (MeV)
^{16}O+^{181}Ta	84	2.1	99.9	50.7
α+^{197}Au	40	35.0	99.9	36.4
α+^{159}Tb	40	28.3	99.5	37.3
α+^{197}Au	50	45.9	99.9	45.9
α+^{116}Sn	50	27.0	99.5	47.6
α+^{nat}Ag	50	24.2	99.5	50.0
α+^{59}Co	50	47.7	99.5	50.5

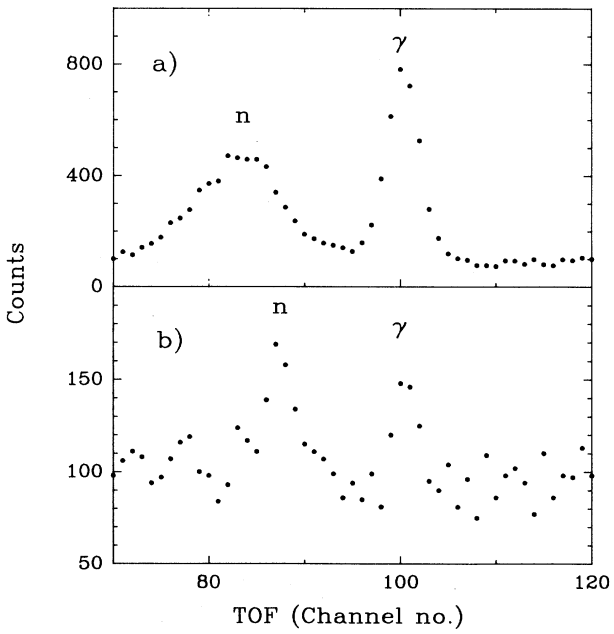

FIG. 1. Typical time-of-flight (TOF) spectra for energy windows (a)18.7$\leq E \leq$21.3 MeV and (b) 28.0 $\leq E \leq$ 32.1 MeV measured in the reaction α+^{197}Au at E_α = 50 MeV.

was found to be less than 5% of yield from the target in the energy region of interest. Further details of the experimental setup were discussed elsewhere [22].

III. EXPERIMENTAL RESULTS

A. Singles measurements and statistical model analysis

The measured singles γ-ray spectra for different targets at E_α =40 MeV and 50 MeV are shown in Fig. 2. All these spectra show the characteristic isovector GDR bump followed by an exponential tail (UDR) with a slope roughly independent of target. Also shown in Fig. 2(c) is a γ-ray spectrum measured in the reaction ^{16}O+^{181}Ta at a beam energy of 84 MeV which populates a similar compound nucleus (at a slightly higher excitation energy) as in the α+^{197}Au case at E_α=50 MeV (Table II). This measurement was made using the ^{16}O beam from the 14UD Pelletron accelerator at Bombay. A comparison of the two spectra provides an empirical evidence for the nonstatistical nature of UDR in α+^{197}Au system since

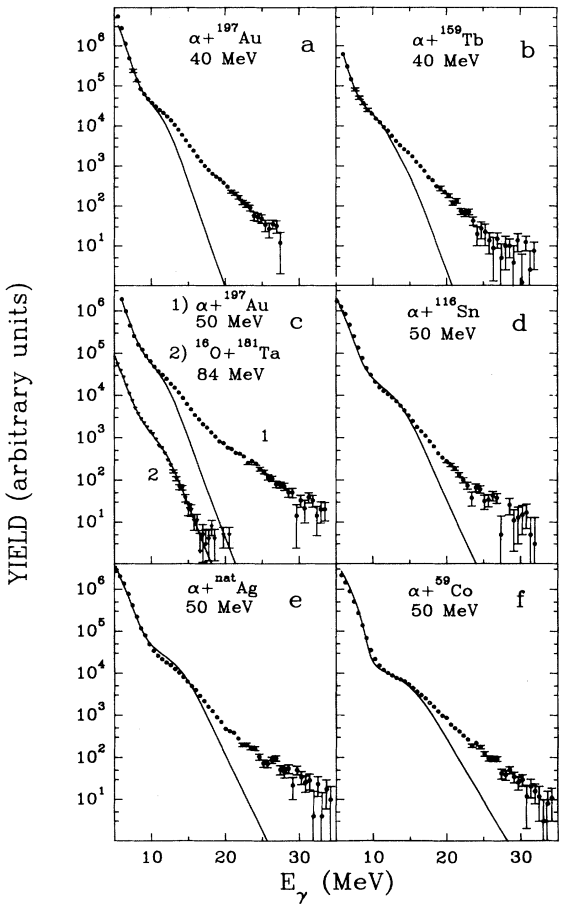

FIG. 2. Measured γ-ray spectra at θ_γ = 90°. Solid lines show the statistical model fits using the code CASCADE (with the parameters given in Table II) after folding with the detector response function.

TABLE II. Parameters used in statistical model calculations. σ_{fus} is the fusion cross section, l_{max} is the maximum angular momentum of the compound nucleus, and X_{FACT} is multiplying factor to get the absolute fit in the lower energy part of the spectra.

Reaction	E^* (MeV)	σ_{fus} (mb)	l_{max}	E_{GDR}[a] (MeV)	Γ_{GDR}[a] (MeV)	X_{FACT}[b]
^{16}O +^{181} Ta	50.7	200	20	13.0	6.0	-
α +^{197} Au	36.4	1108	17	13.0	5.5	0.66
α +^{159} Tb	37.3	1300	17	12.1/15.7	4/6	1.10
α +^{197} Au	45.9	1400	21	13.0	6.0	0.93
α +^{116} Sn	47.6	1300	21	15.2	6.8	1.12
α +^{nat} Ag	50.0	1300	20	15.5	7.0	1.06
α +^{59} Co	50.5	1100	18	17.0	8.5	0.60

[a]Prolate deformation used in the case of α +^{159} Tb, resulting in the split resonance with the two values of E_{GDR} and Γ_{GDR} shown.

[b]The factor deviates from 1.0 beyond the experimental uncertainties only in the case of α+^{59}Co. No obvious reasoning for this can be provided. It may be mentioned that a similar difficulty in fitting the γ-ray spectrum in the reaction α+^{59}Co at E_α=28.4 MeV has also been reported in Ref. [17].

the γ-ray spectrum in the reaction ^{16}O+^{181}Ta can be explained by statistical model calculations in the entire energy range (shown by the solid line). For this calculation we have used a modified version of the code CASCADE [23] with the relevant parameters shown in Table II.

Similar statistical model calculations have been done for all the other α-induced reactions and are shown in Fig. 2 by the solid lines after folding the calculated spectra with the detector response function. For the statistical model calculations the important inputs are the level density, the GDR parameters, and the fusion cross sections. In all these calculations the level density prescription of Reisdorf [24] has been used. The GDR strength has been fixed at 100% of the classical sum-rule strength. The choice of GDR parameters is guided by the systematics in literature [17,25]. The best fit values are obtained by varying these parameters within a reasonable range in order to describe the shape and magnitude of the low energy part of the γ-ray spectra. The input fusion cross sections are either experimental [26,27] or those obtained from semiclassical estimates. All the relevant parameters used in the statistical model calculations have been listed in Table II. The absolute magnitudes of the measured cross sections agree reasonably well (described by X_{FACT} in Table II) with the statistical model below the GDR region except for ^{59}Co.

As can be seen from Fig. 2, the statistical model calculations underestimate the measured γ-ray yields in the UDR region for the α-induced reactions. This observation is independent of the choice of level density parameters within reasonable limits. The inclusion of the isovector giant quadrupole resonance with 100% classical sum-rule strength also does not alter this conclusion in any significant manner. This implies a nonstatistical UDR component in the γ-ray spectrum for all the α-induced reactions as mentioned earlier. From the measured γ-ray yields, the energy differential cross sections have been

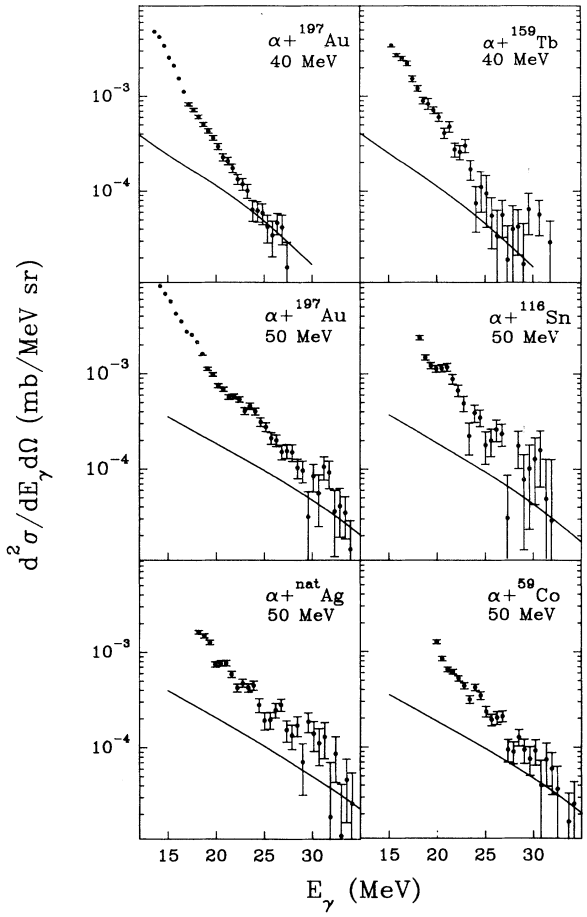

FIG. 3. Excess γ-ray cross sections over the statistical model predictions as a function of E_γ at $\theta_\gamma = 90°$. Errors shown in the figure are statistical only and do not include systematic uncertainties. Solid lines are the sum of the calculated cross sections from the PB and the NNB mechanisms. A sharp-cutoff approximation ($k_F^T = 1.36$ fm^{-1}) is used for the momentum distribution of target nucleons in the NNB calculations (see text).

obtained after unfolding the γ-ray spectra using an iterative technique [22]. The excess cross sections over those calculated from the statistical model are shown for all the targets in Fig. 3. The errors shown in the figure are statistical and do not include systematic uncertainties which could be $\pm$20% for reactions with 50 MeV α beam on ^{197}Au, ^{nat}Ag, and ^{59}Co targets and up to $\pm$40% for the rest.

The energy dependence of the UDR cross sections can be approximated by an exponential, viz., $\exp(-E_\gamma/E_0)$, for $E_\gamma \gtrsim$20 and 25 MeV at E_α = 40 and 50 MeV, respectively. The slope parameters E_0 extracted from the 90° data (Fig. 3) are listed in Table III. Also shown in the table are the energy-integrated cross sections for $E_\gamma \geq$25 and 30 MeV. These are obtained by summing the experimental UDR differential cross sections at 90° up to the highest E_γ^{max} measured, adding a contribution beyond E_γ^{max} from the integral of the extrapolated exponential tail and finally multiplying by 4π.

B. Coincidence measurements

γ-ray spectra measured in coincidence with the multiplicity detectors are found to be essentially similar to the singles spectra for all the reactions studied. The ratio of the coincidence to singles yields in the main detector, which is proportional to the mean γ-ray multiplicity, is shown as a function of γ-ray energy in Fig. 4. The mean multiplicity remains roughly constant over a wider range of E_γ for ^{59}Co compared to that for the heavier targets. This is consistent with the fact that for ^{59}Co the statistical model fits the data up to higher E_γ compared to the rest. In the UDR region there is a general decrease (up to ~30%) of the mean multiplicity with E_γ in all the cases, which suggests that the highest energy γ rays arise from more central collisions.

C. Angular distributions

The γ-ray yields have been measured for the reactions α+^{197}Au and α+^{59}Co at E_α=50 MeV at the laboratory angles of 45°, 90°, and 135° with respect to the beam direction. The ratios of the yields at 45° (R45) and 135° (R135) with respect to those at 90° are shown in Fig. 5 as a function of γ-ray energy . Before calculating the ratios the data have been binned to ~1 MeV and ~2 MeV intervals for $E_\gamma \leq$17 MeV and $E_\gamma >$17 MeV, respectively. The measured ratios are normalized at 9.3 MeV and 12.3 MeV for ^{197}Au and ^{59}Co, respectively, to the values obtained assuming isotropy in the rest frame of the compound nu-

TABLE III. Slope parameters (E_0), integrated cross sections (σ_γ), and the probability (P_γ) per n-p collisions [2] extracted from the UDR spectra. $\sigma_\gamma(>E)$ is 4π times the integral cross section at 90° for $E_\gamma \geq E$.

Reaction	E_{beam} (MeV)	E_0 (MeV)	σ_γ(>25 MeV) (μb)	P_γ(>25 MeV) $\times 10^6$	σ_γ(>30 MeV) (μb)	P_γ(>30 MeV) $\times 10^6$
α + ^{197} Au	40	2.8 ± 0.2	2.0 ± 0.3	0.7 ± 0.1	-	-
α + ^{159} Tb	40	2.7 ± 0.3	4.0 ± 0.8	1.5 ± 0.3	0.9 ± 0.4	0.4 ± 0.2
α + ^{197} Au	50	3.9 ± 0.6	14.5 ± 1.0	4.8 ± 0.3	4.5 ± 0.8	1.5 ± 0.3
α + ^{116} Sn	50	3.6 ± 0.6	13.2 ± 2.2	6.3 ± 1.1	4.4 ± 1.6	2.1 ± 0.8
α + ^{nat} Ag	50	4.4 ± 0.8	17.5 ± 1.6	8.8 ± 0.8	6.1 ± 1.4	3.0 ± 0.7
α + ^{59} Co	50	3.9 ± 0.5	13.1 ± 1.0	9.9 ± 0.8	3.7 ± 0.7	2.8 ± 0.6

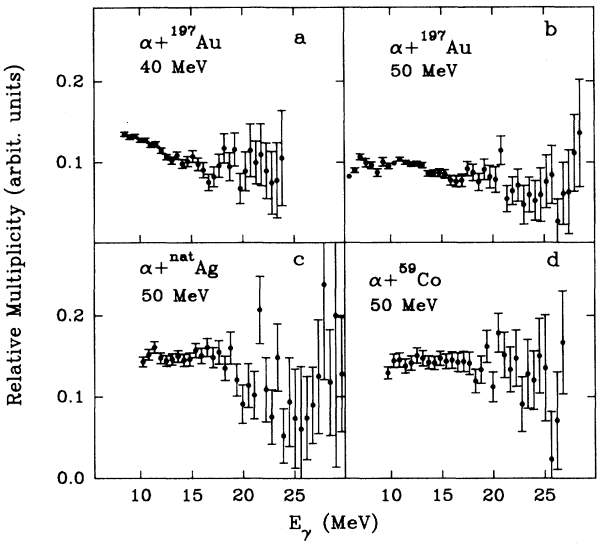

FIG. 4. Relative γ-ray multiplicity (in arbitrary units) obtained from the ratios of the trigger-gated and singles γ-ray yields as a function of E_γ.

cleus and incorporating the appropriate Doppler shifts. The normalization factors are 1.35 and 1.10 for R45 and R135, respectively, for ^{197}Au and 1.48 and 1.05 for ^{59}Co. The calculated asymmetry in the γ-ray angular distribution from the compound nuclear decay is $\leq$5% for ^{197}Au and $\leq$10% for ^{59}Co over the entire γ-ray energy range. Fig. 5 shows that the experimental asymmetries increase with γ-ray energy and are much greater than those predicted by these calculations.

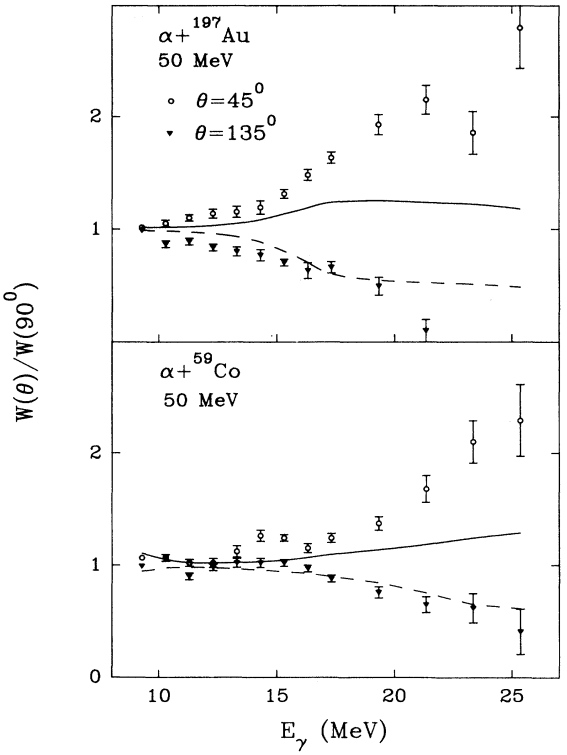

FIG. 5. Ratio of the γ-ray yields (i) $W(45°)/W(90°)$ and (ii) $W(135°)/W(90°)$ as a function of E_γ. The solid and the dashed lines show the calculated anisotropies (i) and (ii), respectively, from the statistical+PB+NNB processes after folding with the detector response function.

IV. BREMSSTRAHLUNG CALCULATIONS

The typical characteristics of the nonstatistical UDR spectra, viz., an approximate exponential shape with a slope parameter of $\sim \frac{1}{3}(E/A)_{\rm beam}$ and large angular asymmetries, are similar to those observed at higher beam energies [1,2]. In view of the reasonable success of the nuclear bremsstrahlung models in explaining these high energy data, an attempt has been made to interpret the present UDR spectra in terms of such a mechanism. There are basically two different models in this class: (i) potential bremsstrahlung model, in which the projectile nucleus radiates as a result of acceleration in the nuclear field of the target and (ii) nucleon-nucleon bremsstrahlung model in which the photons are emitted mainly from collisions between the projectile and the target nucleons. Nakayama and Bertsch [7] argue that at low incident energies the potential bremsstrahlung should be important, particularly near the kinematic limit, i.e., $E_\gamma^{\rm max} = E_{\rm CM} + Q_0$, where Q_0 is the ground-state Q value.

A. Potential bremsstrahlung (PB)

In our calculation we have used the classical bremsstrahlung formula [28] in which the emission probability is written as

$$\frac{d^2P}{dE_\gamma d\Omega} = \frac{e_{\rm eff}^2}{4\pi^2\hbar c E_\gamma}\sum_\epsilon \left| \frac{\mathbf{v}_i\cdot\boldsymbol{\epsilon}}{1-\mathbf{v}_i\cdot\hat{\mathbf{k}}} - \frac{\mathbf{v}_f\cdot\boldsymbol{\epsilon}}{1-\mathbf{v}_f\cdot\hat{\mathbf{k}}}\right|^2, \quad (1)$$

where $\mathbf{v}_i$ and $\mathbf{v}_f$ are the velocities (in units of c) of the projectile outside and inside the target potential, $\boldsymbol{\epsilon}$ is the photon polarization, $\hat{\mathbf{k}}$ is the unit vector in the direction of the photon momentum, E_γ is the photon energy, and $e_{\rm eff}$ is the effective charge of the projectile-target system given by

$$e_{\rm eff} = eA_p\left(\frac{Z_p}{A_p} - \frac{Z_t}{A_t}\right), \quad (2)$$

where $Z_{p(t)}$ and $A_{p(t)}$ are the proton and nucleon number of the projectile (target). The cross section is calculated by integrating the emission probability over impact parameters. Although the classical formula is expected to fail near the kinematic limit, we find that our results agree to within 30% with the one-dimensional quantum mechanical calculation of Ref. [7] up to $E_\gamma \sim 0.8E_\gamma^{\rm max}$ which is higher than the maximum E_γ measured in all the present cases. In the PB calculation of Nakayama and Bertsch [7,18] the Coulomb interaction between the projectile and the target has been neglected. However the Coulomb repulsion slows down the projectile as it approaches the target. This should lead to a larger ac-

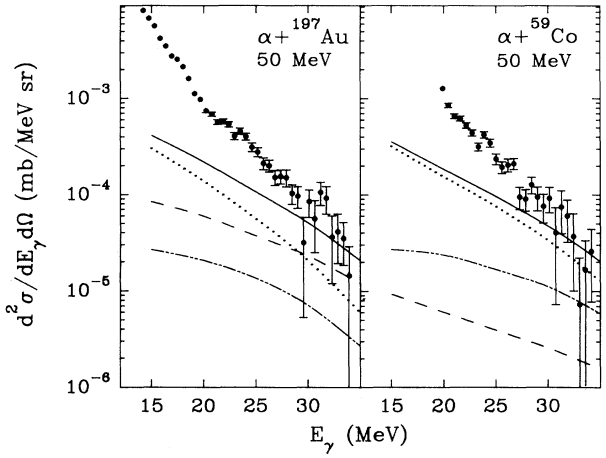

FIG. 6. Calculated cross sections from PB (dashed), NNB-convective (dotted), NNB-exchange (dash-dotted) processes, and their sum (solid), shown in comparison with the data at θ_γ=90°. A sharp-cutoff approximation (k_F^T = 1.36 fm^{-1}) is used for the momentum distribution of target nucleons in the NNB calculations.

celeration once the nuclear potential is felt and, hence, to a larger PB yield. On the other hand the deflection in the Coulomb field for nonzero impact parameters reduces the radial component of the projectile velocity. This lowers the maximum impact parameter that can contribute to the PB yield for a given E_γ leading to a lower cross section. We find that the two effects almost cancel one another at low energy ($E_\gamma \leq$15 MeV). However, at higher γ-ray energies the first effect dominates leading to an overall increase in the UDR cross section. For $E_\gamma \sim$ 35 MeV this increase is about 40% and 15% in the case of ^{197}Au and ^{59}Co, respectively.

The results of our PB calculation including the Coulomb effect for the ^{197}Au and ^{59}Co targets at E_α=50 MeV and $\theta_\gamma = 90°$ are shown in Fig. 6 by dashed curves. A potential depth of 100 MeV is used in these calculations. (Decreasing the potential depth to 50 MeV, for example, reduces the cross sections by a factor of 2 to 3.) As can be seen in the figure the calculated cross section is about half the measured cross section in the case of ^{197}Au at ~34 MeV but further underestimates the data at lower γ-ray energies. However, the PB cross section is negligible in the case of ^{59}Co mainly due to the much smaller effective charge. In Table IV we have listed the calculated cross sections and the maximum impact parameters (b_m) for different γ-ray energies, for all the targets. A comparison of these cross sections and their Z dependence show that the PB mechanism cannot be the only source of the UDR for the reactions studied. A mechanism of enhancing the PB yield would be to include a resonance in the α-nucleus final state. Such a mechanism would show up as a structure in γ-ray yield at $E_{\rm beam} - E_R$, where E_R is the resonance energy of the alpha particle in the compound system. From our data, particularly for α+^{197}Au and α+^{116}Sn at E_α=50 MeV, possible indications of such structures at E_γ ~24 and 21 MeV, respectively, are seen in Figs. 2 and 3. While a suitable choice of energy and width of the resonance can give an enhancement [29] in the resonance region leading to a better agreement with data for the ^{197}Au target, this mechanism cannot explain the data on the lighter targets.

B. Nucleon-nucleon bremsstrahlung (NNB)

The incoherent nucleon-nucleon bremsstrahlung has been found to be an important mechanism for producing high energy γ rays in heavy ion collisions at $E/A \geq$ 20 MeV. The dominant contribution comes from the neutron-proton collisions. The higher energy part of the gamma spectrum ($E_\gamma > E/2A$) arises in this model as a consequence of the boost in the effective collision energy due to the Fermi motion of nucleons in the target and the projectile. The general decrease of cross section with E_γ comes mainly from the Pauli blocking in the final state of the colliding nucleons which becomes more effective as the γ-ray energy increases. In a complete treatment of the problem one should follow the evolution of the phase space distribution of the projectile and target nucleons. Photon emission is possible at all stages of the collision. However, it has been argued that the dominant contribution to photon emission is from the first chance neutron-proton collisions [2]. At our energies this should be a good approximation. We have followed the prescription of Nakayama and Bertsch [7,19] to calculate the UDR cross section in the alpha induced reactions. Our motivation in these calculations is to find out how far this model can work at low beam energies. This would bring into focus some subtleties which are probably not important at higher beam energies.

In this first chance collision model the calculation is done in the momentum space. Nucleons in the projectile

TABLE IV. Calculated γ-ray cross sections in nb MeV^{-1} sr^{-1} and the maximum impact parameters in fm (in parentheses) at $\theta_\gamma = 90°$ in the PB model.

E_γ (MeV)	^{197}Au (40 MeV)	^{159}Tb (40 MeV)	^{197}Au (50 MeV)	^{116}Sn (50 MeV)	^{nat}Ag (50 MeV)	^{59}Co (50 MeV)
15	72.3(4.6)	60.7(4.7)	79.0(5.2)	32.6(5.1)	28.4(5.1)	9.5(4.7)
20	54.2(4.6)	40.9(4.5)	59.2(5.2)	20.7(4.7)	19.2(4.8)	6.0(4.3)
25	29.6(3.8)	22.6(3.8)	37.4(4.7)	13.2(4.2)	12.4(4.4)	3.9(3.9)
30	13.6(2.9)	11.0(2.9)	22.9(4.0)	8.4(3.7)	8.0 (3.9)	2.6(3.5)
35	2.4 (1.3)	2.9 (1.6)	13.2(3.3)	5.1(3.1)	5.1 (3.4)	1.6(3.0)

with their internal momentum distribution, collide with nucleons in the target, which is treated as nuclear matter characterized by the Fermi momentum k_F^T. The cross section for gamma production is written as a product of (1) the probability of γ-ray production in the basic n-p collision, (2) the weighted average number of n-p pairs in each projectile nucleon-target nucleon collision (N_{np}), and (3) the total reaction cross section(σ_R) as

$$\frac{d^2\sigma}{dE_\gamma d\Omega} = \sigma_R N_{np} \frac{d^2P}{dE_\gamma d\Omega} , \tag{3}$$

where

$$\sigma_R = \pi R^2 \left(1 - \frac{V_c}{E_{cm}}\right) , \tag{4}$$

$$V_c = 1.44 Z_p Z_t / R \text{ (MeV)} , \tag{5}$$

$$R = 1.4(A_p^{1/3} + A_t^{1/3}) \text{ (fm)}, \tag{6}$$

and

$$N_{np} = \frac{(Z_p N_t + Z_t N_p)\sigma_{np}}{(Z_p N_t + Z_t N_p)\sigma_{np} + Z_p Z_t \sigma_{pp} + N_p N_t \sigma_{nn}} . \tag{7}$$

Here $Z_{p(t)}$ and $N_{p(t)}$ denote the proton and neutron numbers of the projectile (target) and σ_{np}, etc., are the two-body collision cross sections. Assuming $\sigma_{np} = 3\sigma_{pp} = 3\sigma_{nn}$ (a valid approximation in the range of collision energies relevant in the present case) and noting that the projectile in the present case is self-conjugate, one gets $N_{np} = 0.75$. The relative probability of gamma emission is given by

$$\frac{d^2P}{dE_\gamma d\Omega} = \frac{d^2W_{pn\gamma}}{dE_\gamma d\Omega} \frac{1}{W_{pn}}, \tag{8}$$

where the $W_{pn\gamma}$ and W_{pn} are proportional to the γ-ray production rate in n-p collisions and the n-p collision rate, respectively. These are calculated using the square of the basic $np\gamma$ and np matrix elements and folding them over the momentum distribution of the target and projectile nucleons, taking into account the Pauli blocking in the final state. It should be noted that in the convective process [see Eq. (10) below] there is no spin-isospin flip of the nucleons implying that the Pauli blocking in the α particle should not be considered. The exchange contribution [see Eq. (11) below] for which there may be spin-isospin flip and hence the need for Pauli blocking, is, however, relatively less important in the present cases. Moreover, as discussed below, the internal momentum distribution of the nucleons in the α particle is very diffuse. Therefore, in all the calculations the Pauli blocking in the projectile has been neglected. The numerical integrations were performed by the Monte Carlo technique.

The photon emission amplitude in the basic n-p collision is written as a sum of three terms, viz.,

$$V_{\rm em} = V_{\rm conv} + V_{\rm magn} + V_{\rm exch}. \tag{9}$$

Here $V_{\rm conv}$ stands for the convective current, $V_{\rm magn}$ for the magnetization current, and $V_{\rm exch}$ for the exchange current contributions. These amplitudes, calculated in the soft photon limit, are expressed by Nakayama and Bertsch in terms of the energy-dependent T matrices [19]. The energy dependence (both on $E_{\rm c.m.}$ and E_γ in the n-p center of mass) has been parametrized and tabulated in Refs. [19,30]. In our calculations the magnetization contribution has been neglected in order to save computational time, since it is checked to be small (<5%). The matrix elements for the convective and the exchange terms are written, following Ref. [19], as

$$\langle \epsilon, \mathbf{k}; \mathbf{p}' S' M' | V_{\rm conv} | 0; \mathbf{p} S M \rangle = \left(\frac{2\pi}{k}\right)^{1/2} \frac{e}{E_\gamma} T_{\rm conv}(E_{\rm c.m}, E_\gamma) \delta_{SS'} \delta_{MM'} \left(\frac{\mathbf{v}\cdot\epsilon}{1 - \mathbf{v}\cdot\hat{\mathbf{k}}} - \frac{\mathbf{v}'\cdot\epsilon}{1 - \mathbf{v}'\cdot\hat{\mathbf{k}}} \right) , \tag{10}$$

$$\langle \epsilon, \mathbf{k}; \mathbf{p}' S' M' | V_{\rm exch} | 0; \mathbf{p} S M \rangle$$

$$= 2e \left(\frac{2\pi}{k}\right)^{1/2} \left(\frac{f}{\mu}\right)^2 \frac{1}{q^2 + \mu^2} \left\langle S' M' \left| \left[2\epsilon\cdot\mathbf{q} \frac{\boldsymbol{\sigma}_1\cdot\mathbf{q}\boldsymbol{\sigma}_2\cdot\mathbf{q}}{q^2+\mu^2} - (\boldsymbol{\sigma}_1\cdot\epsilon\boldsymbol{\sigma}_2\cdot\mathbf{q} + \boldsymbol{\sigma}_1\cdot\mathbf{q}\boldsymbol{\sigma}_2\cdot\epsilon) \right] \right| SM \right\rangle . \tag{11}$$

The momenta $\mathbf{p}$ and velocity $\mathbf{v}$ (the primed quantities in the final state) correspond to those in the n-p center-of-mass frame and are obtained by suitable relativistic transformations. σ_1 and σ_2 are the Pauli spin matrices, S and M are the total spin and its projection, $\mathbf{q}$ is the momentum transfer, and k is the magnitude of the photon momentum. The amplitudes $T_{\rm conv}$ and $(f/\mu)^2$ relevant for the convective and exchange contributions are calculated from the parametrizations in Ref. [30].

The nucleon momentum distribution in the target is assumed to be constant up to a maximum value k_F^T. The distribution of internal momentum $k_{\rm int}$ of the nucleons inside the alpha particle has been parametrized [31] as

$$P(k_{\rm int}) = \frac{1}{1 + \exp\left[(k_{\rm int} - k_1)/a\right]}, \tag{12}$$

with $k_1 = 0.4$ fm^{-1} and $a = 0.2$ fm^{-1}. In the calculations involving high energy projectiles the effective momentum k_i of the projectile nucleon in the target rest frame is usually taken as $k_i = k_{\rm beam} + k_{\rm int}$, $k_{\rm beam}$ being the wave vector of a nucleon with energy $E_{\rm beam}/A$. A better prescription should take into account the mean field seen by the projectile nucleons in the target, viz., $k_i = k'_{\rm beam} + k_{\rm int}$ where, $k'_{\rm beam}$ is the wave vector corresponding to the energy $[(E_{\rm beam}/A) + E_F^T + Q_0/4]$ where E_F^T is the Fermi energy in the target. Here $E_F^T + Q_0/4$ is the effective mean

field potential for the projectile nucleon. Further the maximum energy $E_{\max}$ available to the nucleon for collision is limited to $E_{\max} = E_{\text{beam}} + E_F^T + Q_0$ in which case the other three nucleons are at the top of the target Fermi sea. Such a limit is not important in high energy heavy ion collisions. In the present Monte Carlo calculation we sample over the one-nucleon momentum distribution in the α particle without ensuring, however, that all the four nucleon momenta add to zero in the projectile frame. A sample calculation, in which the momentum conservation together with the condition that all the four particles are above the Fermi sea in the target was implemented, shows that the γ-ray cross section reduces to $\sim$70 % for all γ-ray energies but does not change the angular distribution. The choice of the Fermi momentum k_F^T for the target in these calculations is not very clear. This can be taken as the nuclear matter value of 1.36 fm^{-1} if the collision takes place in the volume of the target. This may not be realistic if the collision takes place at the surface, in which case a lower value may be relevant because of the lower local density. In order to estimate the effect of k_F^T on the UDR cross section, we have made calculations for k_F^T =1.36 and 1.0 fm^{-1}, corresponding to about 1.0 and 0.4 times, respectively, the saturation (nuclear matter) density. It should be noted that in our method a decrease in k_F^T also decreases the effective mean field potential. The comparison for the above two choices of k_F^T shows that the slopes of the cross sections are almost the same and the magnitude decreases by about 30% for the lower k_F^T value. The results of the NNB calculations for α+^{197}Au and α+^{59}Co systems at E_α=50 MeV and $\theta_\gamma = 90°$ are shown in Fig. 6 for k_F^T=1.36 fm^{-1}. The convective and exchange contributions to the UDR cross section have been shown separately by the dotted and the dash-dot-dash lines. The exchange term contributes $\sim$ 10% to 35% for E_γ = 15 MeV to 35 MeV. As seen in the figure neither PB nor NNB can explain the data. While it is not clear whether these two processes are independent, a sum of the two contributions is shown by the solid lines in Fig. 6 and also, for all the cases studied, in Fig. 3. In order to compare the experimental angular distributions with the calculations, the statistical, PB and NNB cross sections were summed and folded with the detector response functions at each measured angle. These were then binned into the experimental steps before taking the ratios (see Fig. 5). It is seen from Figs. 3 and 5 that (1) the calculated cross sections systematically underpredict the data by a factor ranging from $\sim$ 5 to $\sim$ 2 for $E_\gamma \sim$ 20 to 34 MeV for all targets and (2) the energy variation of the calculated anisotropies cannot reproduce the data. The failure in understanding the angular distributions can well be related to the incorrect prediction of the UDR cross sections. We have also relaxed the sharp-cutoff approximation for the momentum distribution of the target nucleons in the NNB calculation. The results of such calculations with a realistic momentum distribution [32] are shown in Fig. 7. The overall UDR cross section increases but the predicted fall of the cross section with E_γ is very slow leading to an overestimation at the highest γ-ray energies. Also the calculated angular anisotropies still fail to reproduce the data.

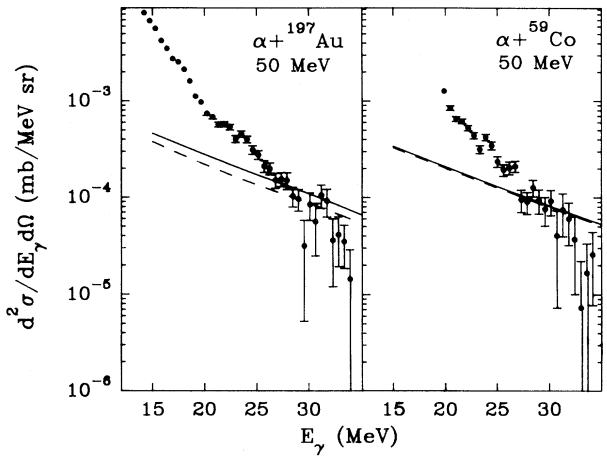

FIG. 7. Calculated cross sections from NNB (dashed) process using a realistic momentum distribution for the target nucleons, and PB+NNB (solid) processes, shown in comparison with the data at $\theta_\gamma = 90°$.

At this point it may be worthwhile to extract the "experimental" values of the probability of gamma emission per n-p collision and compare with the systematics derived from the higher energy data as shown in Fig. 14 of Ref. [2]. For this the integral cross sections above E_γ =25 and 30 MeV are divided by $N_{np}\sigma_R$ as defined in the above reference. These are shown in the last two columns of Table III. Compared to the above systematics the present values are about a factor of 3 to 10 higher. This also probably signifies the failure of the NNB model for describing the low energy data.

Another attempt to calculate the high energy photon spectrum is made by folding the experimental p nucleus γ-ray spectra over the effective nucleon energies in the projectile. In this procedure the effect of folding the elementary $np\gamma$ cross section over the momentum distribution of the target nucleons is empirically included. However, the shortcoming in this approach is the lack of low energy p nucleus γ-ray cross sections. We have parametrized the data available at 72, 104, 145, 168, and 200 MeV proton energies [33–35] as

$$\frac{d^2P}{dE_\gamma d\Omega} = A \exp\left(-\frac{x}{a}\right) f(x), \tag{13}$$

with the differential cross section given in Eq. (3). Here $x = E_\gamma/E_1$, $E_1 = E_p + S_p$, E_p, S_p being the incident energy and the proton separation energy, respectively. The beam energy dependence of the parameters A, a and the function $f(x)$ are expressed as

$$\begin{aligned} A &= (2.05 + 0.003\ E_1) \times 10^{-6}\ \text{MeV}^{-1}\,\text{sr}^{-1}\ , \\ a &= 0.24\ , \\ f(x) &= 1,\ x < x_0 \\ &= 1.0 - m\ (x - x_0),\ x > x_0\ , \\ x_0 &= 0.5\ , \\ m &= (1.67 + 0.006\ E_1) \quad (m \geq 2)\ . \end{aligned} \tag{14}$$

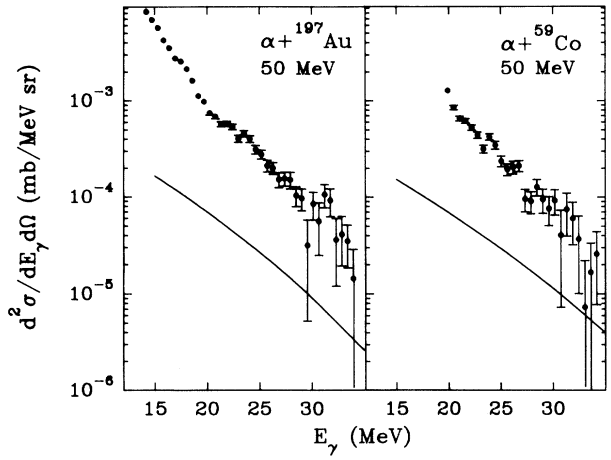

FIG. 8. α-nucleus γ-ray cross sections calculated by folding the p nucleus γ-ray cross sections described by the parametrization in the text, shown in comparison with the data at $\theta_\gamma = 90°$.

The above parametrization reproduces the p-nucleus data at $\theta_\gamma = 90°$ for $E_\gamma \gtrsim 30$ MeV. While folding the p-nucleus cross section, we calculate the momentum of the projectile nucleons by adding the internal nucleon momentum to the beam momentum per nucleon. The nucleon momentum distribution inside the alpha is assumed as given in Eq. (12) above. The nucleon energy calculated from the resultant momentum becomes the effective incident energy. This is taken as E_1 in the above equations after neglecting the effective separation energy $S = Q_0/4$. The upper limit on the projectile nucleon momentum is decided by $(\sqrt{E_{\rm beam}} + \sqrt{E_{\rm int}})^2$ or $E_{\rm c.m.} + Q_0$ whichever is lower, and the lower limit, by $(\sqrt{E_{\rm beam}} - \sqrt{E_{\rm int}})^2$ or E_γ whichever is higher. Here $E_{\rm int}$ is the internal kinetic energy of the nucleon in the alpha, $E_{\rm c.m.}$ is the energy in the α nucleus center-of-mass system. Another assumption made for simplicity is the isotropy of the p nucleus γ-ray cross section. Figure 8 shows the results of these calculations. The calculated cross sections are about an order of magnitude lower than experiment for $E_\gamma \sim 20$ to 35 MeV. However, the above parametrization of the p nucleus UDR data at 90° for E_γ in the 20 to 30 MeV region is not good (data up to a factor of 2.5 to 1.6, respectively, higher than that given by the above parametrization). In addition, the angular distribution effects could bring another factor of 1.5 to 2.5. Finally, the preliminary measurements of Gossett *et al.* [36] at E_p=33.5 MeV shows the γ-ray cross sections to be ~4 to 5 times more than our parametrized values. All these factors may lead to an order of magnitude enhancement of the calculated cross sections, and hence, to a reasonable agreement with the data.

V. SUMMARY AND CONCLUSIONS

We have measured α-induced photon spectra for E_γ ~5 to 35 MeV in α+^{159}Tb and ^{197}Au at E_α=40 MeV and α+^{59}Co, $^{\rm nat}$Ag, ^{116}Sn, and ^{197}Au at E_α=50 MeV. The low energy part of the spectra for $E_\gamma \lesssim E_{\rm GDR}$ agrees reasonably with the statistical model and shows a large excess in the UDR region, viz., $E_\gamma > E_{\rm GDR}$. For E_α=50 MeV the integral γ-ray cross section (E_γ >25 MeV) is approximately independent of the target and is between 13 and 17.5 μb. The relative photon multiplicity associated with UDR emission reduces by about 30% from the lowest to the highest γ-ray energies. The angular distributions measured at E_α=50 MeV for ^{59}Co and ^{197}Au show near isotropy for $E_\gamma \lesssim E_{\rm GDR}$ and an asymmetry which increases with E_γ in the UDR region. At the highest E_γ the ratio $W(45°)/W(90°)$ and $W(135°)/W(90°)$ is ~2.0 and 0.6, respectively, for both the targets. We have performed PB and NNB calculations for all the reactions studied. The PB calculations show a strong target dependence due to the large variation in the effective charge from ^{59}Co to ^{197}Au, at variance with our data. Even for the case of α+^{197}Au, where the PB gives the largest contribution the calculated cross section is ~50% of the experimental cross section at $E_\gamma \sim 34$ MeV. The NNB calculations were done following Nakayama and Bertsch where only the first chance n-p collisions were considered. Using a realistic momentum distribution for nucleons in the α particle and a flat Fermi distribution (with $k_F^T = 1.36$ fm^{-1}) for nucleons in the target gives a cross section which is ~5 to 2 times smaller than the experiment in the UDR region for $E_\gamma \sim 20$ to 34 MeV, respectively. Using a realistic momentum distribution for the target increases the cross section. However, the calculated spectrum is even harder, underpredicting the data by $\sim$ 3.6 at E_γ =20 MeV and overpredicting the data by $\sim$ 3.0 at E_γ =34 MeV. Also the calculated angular distributions remain essentially the same for the flat or the realistic momentum distribution in the target and gives the ratio $W(45°)/W(90°)$ which is less strongly varying with E_γ as compared to the data. The ratio $W(135°)/W(90°)$ roughly agrees with the experiment. A separate calculation has been done folding the experimental p nucleus γ-ray cross sections over the momentum distribution of the projectile nucleons. While this procedure seems to give the cross sections of the right order, one should reserve judgment about the success of these calculations due to the paucity of low energy p nucleus data.

In conclusion, the potential and the nucleon-nucleon bremsstrahlung calculations fail to reproduce the γ-ray cross sections in the full UDR region and also the angular distributions. There is a need for more low energy p nucleus data in order to judge whether a folding approach works for α-induced bremsstrahlung where the Pauli blocking for the projectile should not be important.

ACKNOWLEDGMENTS

The authors wish to thank H.C. Jain, A. Roy, M. Dasgupta, R. Varma, D.A. Gothe, and M.T. Gaekwad for their help during the experiments. The excellent cooperation of S.N. Chintalapudi and the staff at the Variable Energy Cyclotron Centre, Calcutta, is acknowledged. We are grateful to C.S. Warke and V.R. Pandharipande for many illuminating discussions.

[1] H. Nifenecker and J.A. Pinston, Prog. Part. Nucl. Phys. **23**, 271 (1989), and references therein.
[2] H. Nifenecker and J.A. Pinston, Annu. Rev. Nucl. Part. Sci. **40**, 113 (1990), and references therein.
[3] W. Cassing, V. Metag, U. Mosel, and K. Niita, Phys. Rep. **188**, 363 (1990).
[4] K.A. Snover, Annu. Rev. Nucl. Part. Sci. **36**, 545 (1986).
[5] K.A. Snover, Nucl. Phys. **A553**, 153c (1993).
[6] J.J. Gaardhøje, Annu. Rev. Nucl. Part. Sci. **42**, 483 (1992).
[7] K. Nakayama and G.F. Bertsch, Phys. Rev. C **34**, 2190 (1986).
[8] H. Nifenecker and J.P. Bondorf, Nucl. Phys. **A442**, 478 (1985).
[9] D. Vasak, B. Müller, and W. Greiner, J. Phys. G **11** 1309 (1985).
[10] D. Vasak , Phys. Lett. **176B**, 276 (1986).
[11] R. Shyam and J. Knoll, Nucl. Phys. **A448**, 322 (1986).
[12] G. Breitbach, G. Koch, S. Koch, W. Kühn, A. Ruckelshausen, V. Metag, R. Novotny, S. Riess, D. Habs, D. Schwalm, E. Grosse, and H. Ströher, Phys. Rev. C **40**, 2893 (1989).
[13] R.J. Vojtech, R. Butsch, V.M. Datar, M.G. Herman, R.L. McGrath, P. Paul, and M. Thoennessen, Phys. Rev. C **40**, R2441 (1989).
[14] C.A. Gossett, J.A. Behr, S.J. Luke, B.T. McLain, D.P. Rosenzweig, K.A. Snover, and W.T. Hering, Phys. Rev. C **42**, R1800 (1990).
[15] R. Pfaff, B. Young, W. Benenson, J. Clayton, M. Thoennessen, D.J. Morrissey, N.A. Orr, T. Refposeur, and J. Winger, MSU report, 1991.
[16] C.L. Tam, J. Stevenson, W. Benenson, J. Clayton, Y. Chen, E. Kashy, A.R. Lampis, D.J. Morrissey, M. Samuel, T.K. Murakami, and J.S. Winfield, Phys. Rev. C **38**, 2526 (1988).
[17] M. Kicinska-Habior, K.A. Snover, C.A. Gossett, J.A. Behr, G. Feldman, H.K. Glatzel, J.H. Gundlach, and E.F. Garman, Phys. Rev. C **36**, 612 (1987).
[18] K. Nakayama and G.F. Bertsch, Phys. Rev. C **36**, 1848 (1987).
[19] K. Nakayama and G.F. Bertsch, Phys. Rev. C **40**, 685 (1989).
[20] W.R. Nelson, H. Hirayama, and D.W.O. Rogers, SLAC Report No. 265, Stanford Linear Accelerator Center (1985).
[21] A. Bandyopadhyay, A. Roy, S.K. Dey, S. Bhattacharya, and R.K. Bhowmik, Nucl. Instrum. Methods **A257**, 309 (1987).
[22] Y.K. Agarwal, C.V.K. Baba, D.R. Chakrabarty, V.M. Datar, D.A. Gothe, H.C. Jain, A. Roy, and M.K. Sharan, Pramana **35**, 49 (1990).
[23] F. Pühlhofer, Nucl. Phys. **A280**, 267 (1977).
[24] W. Reisdorf, Z. Phys. A **300**, 227 (1981).
[25] D.R. Chakrabarty, S. Sen, M. Thoennessen, N. Alamanos, P. Paul, R. Schicker, J. Stachel, and J.J. Gaardhøje, Phys. Rev. C **36**, 1886 (1987).
[26] J. Jastrzebski, P.P. Singh, T. Mroz, S.E. Vigdor, M. Fatyga, and H.J. Karwowski, Phys. Rev. C **34**, 60 (1986).
[27] H.E. Kurz, E.W. Jasper, K. Fischer, and F. Hermes, Nucl. Phys. **A168**, 129 (1971).
[28] J.D. Jackson, *Classical Electrodynamics* (Wiley, New York, 1975).
[29] Y.K. Agarwal, C.V.K. Baba, D.R. Chakrabarty, M. Dasgupta, V.M. Datar, H.C. Jain, A. Roy, and M.K. Sharan, Proceedings of the International Conference on Nuclear Physics, Sao Paulo, 1989 (unpublished).
[30] V. Herrmann, J. Speth, and K. Nakayama, Phys. Rev. C **43**, 394 (1991).
[31] R. Schiavilla, V.R. Pandharipande, and R.B. Wiringa, Nucl. Phys. **A449**, 219 (1986).
[32] M. Casas, J. Martorell, E. Moya de Guerra, and J. Treiner, Nucl. Phys. **A473**, 429 (1987).
[33] M. Kwato Njock, M. Maurel, H. Nifenecker, J. Pinston, F. Schussler, D. Barneoud, S. Drissi, J. Kern, and J.P. Vorlet, Phys. Lett. B **207**, 269 (1988).
[34] J.A. Pinston, D. Barneoud, V. Bellini, S. Drissi, J. Guillot, J. Julien, M. Kwato Njock, H. Nifenecker, M. Maurel, F. Schussler, and J.P. Vorlet, Phys. Lett. B **218**, 128 (1989).
[35] J. Clayton, W. Benenson, M. Cronqvist, R. Fox, D. Krofcheck, R. Pfaff, T. Reposeur, J.D. Stevenson, J.S. Winsfield, B. Young, M.F. Mohar, C. Bloch, and D.E. Fields, Phys. Rev. C **45**, 1815 (1992).
[36] C.A. Gossett, M.S. Kaplan, S.J. Luke, B.T. McLain, R. Vandenbosch, and D.P. Wells, Nuclear Physics Laboratory Annual Report, University of Washington (1991), p. 14; (1992), p. 17.